

Numerical Investigations on Supersonic Fluid Flow past a Cavity Relating Coefficient of Pressure and Density Fields

Dr. Nirmal Kumar Kund

Associate Professor, Department of Production Engineering, Veer Surendra Sai University of Technology, Burla, Odisha, India

ABSTRACT

A very precise numerical model is developed to work out supersonic flow past a 3D open cavity. The examinations of supersonic flow past the 3D open cavity possessing length-to-depth ratio of 2, comprise the supersonic free-stream Mach number of 2 besides the flow Reynolds number of 10^5 . The numerical simulation has been executed through the Large Eddy Simulation (LES) method. The Smagorinsky model is engaged for this exercise. The simulation predictions have been accessed in the form of both aeroacoustic effect symbolised by the coefficient of pressure (C_p) and the cavity flow-field epitomized by the density contour. The grid independence test relating to the coefficient of pressure has also been accomplished. The LES model enables to estimate all the vital flow behaviors of the open cavity flow. Furthermore, the feedback loop mechanism of the open cavity flow has also been discussed. Very large recirculation is witnessed within the open cavity and therefore these require to be suppressed. Nevertheless, the combination of a spoiler at the leading edge of the open cavity is also planned for the future to alter the flow behaviors within the open cavity, which can also bring about the reduction in the recirculation within the open cavity as well.

Keywords: Numerical Simulation, Open Cavity, LES, Coefficient of Pressure, Density Contour

I. INTRODUCTION

In our everyday life, we feel noise from sources like exhaust pipes, vacuum cleaners, ventilation systems, fans etc. The flow induced noise is a major problem in many engineering applications like military vehicles, submarines, aircrafts, automobiles, etc. Airframe noise is a considerable component of overall noise. One of the most significant airframe noises is the cavity noise. They arise from sources like open wheel wells, weapon bays, door gaps, side mirrors, open sun roof, etc. The door gaps, open wheel wells and weapon bays can be modelled as rectangular cavities and the collected flow external the cavity can be regarded as smooth and even. Though the rectangular cavity is simple in shape, it is very rich in diverse dynamic and acoustic phenomena, obscured by a possible aeroacoustic

feedback loop depending on the shape/size of the cavity as well as the flow conditions. Severe tone noises may be produced because of the vortex shredding at the upstream edge of the cavity during the flow over a cavity.

Heller et al. [1] illustrated on flow-induced pressure oscillations in shallow cavities. Tam and Block [2] studied on the tones and pressure oscillations induced by flow over rectangular cavities. Kaufman et al. [3] reported on Mach 0.6 to 3.0 flows over rectangular cavities. Sweby [4] applied high resolution schemes using flux limiters on hyperbolic conservation laws. Rizzetta [5] performed numerical simulation on supersonic flow over a three-dimensional cavity. Anderson and Wendt [6] described about the fundamentals of computational fluid dynamics. Piomelli [7] demonstrated on

achievements and challenges of large-eddy simulation. Hamed et al. [8] conducted numerical simulations of fluidic control for transonic cavity flows. Li et al. [9] carried out LES study of feedback-loop mechanism of supersonic open cavity flows. Vijayakrishnan [10] executed a validation study on unsteady RANS computations of supersonic flow over two dimensional cavity. Sousa et al. [11] discussed about the lid-driven cavity flow of viscoelastic liquids. Tuerke et al. [12] investigated the experimental study on double-cavity flow. It is realized that an extensive study on cavity flow has been done both experimentally and computationally for improving the aerodynamic performance. However, besides its importance, the complicated flow physics of flow past a cavity has fascinated the investigators for further studies and still continues to be a thrust area of research.

Albeit, the flow over an open cavity has been investigated experimentally/numerically by many researchers, but, complete modelling of both large and small scales of motions altogether, not yet done which is one of the major weaknesses. However, Large Eddy Simulation (LES) is the method which resolves the large eddies as it is and models the small eddies that can give reasonably more realistic results as well. The purpose of this research work is to study the flow physics along with the aeroacoustics in a 3D open cavity supersonic flow. It involves details about the governing equations and the development together with the implementation of the LES technique including the sub-grid scale modelling. The discretization procedures have also been described. The simulation results have been presented in the form of coefficient of pressure (C_p) and density contour. However, the studies pertaining to the use of passive control techniques/devices for the suppression of recirculation within the cavity is also planned for the future. As these devices which operate over a wide range of parameters, significantly affect the flow physics of incoming boundary layer for extending equally effective flow circumstances.

II. DESCRIPTION OF PHYSICAL PROBLEM

Supersonic flow past a three-dimensional cavity is studied numerically. The streamwise length, depth and spanwise length of the cavity are 20 mm, 10 mm, and 10 mm, respectively. The length-to-depth ratio (L/D) for the cavity is 2. The width-to-depth ratio (W/D) is 1. The cavity is three-dimensional with streamwise length-to-spanwise length ratio (L/W) > 1 . In addition, the Mach number of the free-stream along with the Reynolds number based on the cavity depth are taken as 2 and 10^5 , respectively, for setting the inflow conditions.

A. Geometric model

The computational domain of the cavity used in the present simulation is shown in figure 1. The size of the computational domain, as mentioned earlier, is $2D \times D \times D$ (length \times breadth \times width). The inlet boundary is located at a distance of D upstream from the leading edge of the cavity. The outlet boundary is located at a distance of $4D$ downstream from the trailing edge of the cavity. The upper boundary is also located at a distance of $4D$ above the cavity.

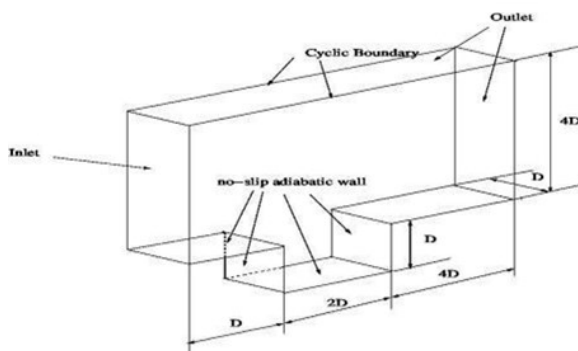


Figure 1. Computational domain of cavity.

B. Initial and boundary conditions

The inflow boundary conditions are initialized with free-stream conditions of $M_\infty = 2$, $P_\infty = 101.325$ kPa, and $T_\infty = 300$ K. The Reynolds number of the flow used in the simulation is 10^5 , which is based on the cavity depth. No-slip adiabatic wall boundary conditions is applied at the wall boundaries. Zero-gradient condition is applied at all the outflow

boundaries. Periodical boundary condition is applied in the spanwise direction of the cavity.

III. MATHEMATICAL FORMULATION

A. Generalized governing transport equations

The three-dimensional compressible Navier-Stokes equations are the governing equations which include the continuity equation (1), the momentum equation (2), and the energy equation (3) which are as follows:

$$\frac{\partial \rho}{\partial t} + \nabla \cdot (\rho \mathbf{U}) = 0 \quad (1)$$

$$\frac{\partial (\rho \mathbf{U})}{\partial t} + \nabla \cdot (\rho \mathbf{U} \mathbf{U}) - \nabla \cdot \nabla (\mu \mathbf{U}) = -\nabla p \quad (2)$$

$$\frac{\partial (\rho e)}{\partial t} + \nabla \cdot (\rho e \mathbf{U}) - \nabla \cdot \nabla (\mu e) = -p(\nabla \cdot \mathbf{U}) + \mu \left[\frac{1}{2} (\nabla \mathbf{U} + \nabla \mathbf{U}^T) \right]^2 \quad (3)$$

Where, \mathbf{U} = velocity vector = $u\hat{i} + v\hat{j} + w\hat{k}$

$\frac{1}{2} (\nabla \mathbf{U} + \nabla \mathbf{U}^T)$ = strain rate tensor.

The equations (1), (2) and (3) represent the conservation form of the Navier-Stokes equations. The conservation form of these governing equations are achieved from a flow model fixed in space [6]. The above equations are applicable to viscous flow, except that the mass diffusion is no included.

It is assumed, in aerodynamics, that the gas is a perfect gas. The equation of state for a perfect gas is,

$$p = \rho RT \quad (4)$$

Where, R = specific gas constant = $C_p - C_v$ (5)

For a calorically perfect gas (constant specific heats), the caloric equation of state is,

$$e = \text{internal energy per unit mass} = C_v T \quad (6)$$

B. LES Turbulence Modelling

The turbulent flows may be simulated using three different approaches: Reynolds-Averaged Navier-Stokes equations (RANS), direct numerical simulation (DNS), and large eddy simulation (LES). Direct numerical simulation has high computational requirements. DNS resolves all the scales of motion and for this it needs a number of grid points proportional to $(\text{Re})^{9/4}$ and computational scales' cost is proportional to $(\text{Re})^3$ [7].

In the present study, features of the turbulent flow field have been simulated using LES as it is appropriate for unsteady complex flows as well as noise induced flows. LES computes the large resolved scales and also models the smallest scales. The turbulence model is introduced by splitting the time and space varying flow variables into two constituents, the resolved one \bar{f} and f' , the unresolved part:

$$f(x,t) = \bar{f}(x,t) + f'(x,t) \quad (7)$$

LES uses a filtering operation to separate these resolved scales from the unresolved scales. The filtered variable is denoted by an over bar [7]. The top-hat filter smooth both the fluctuations of the large-scale and those of small scales as well. The filtering operation when applied to the Navier-Stokes equation gives:

$$\frac{\partial \bar{\rho}}{\partial t} + \nabla \cdot (\bar{\rho} \bar{\mathbf{U}}) = 0 \quad (8)$$

$$\frac{\partial (\bar{\rho} \bar{\mathbf{U}})}{\partial t} + \nabla \cdot (\bar{\rho} \bar{\mathbf{U}} \bar{\mathbf{U}}) - \nabla \cdot \nabla (\bar{\mu} \bar{\mathbf{U}}) = -\nabla \bar{p} \quad (9)$$

$$\frac{\partial (\bar{\rho} \bar{e})}{\partial t} + \nabla \cdot (\bar{\rho} \bar{e} \bar{\mathbf{U}}) - \nabla \cdot \nabla (\bar{\mu} \bar{e}) = -\bar{p}(\nabla \cdot \bar{\mathbf{U}}) + \mu \left[\frac{1}{2} (\nabla \bar{\mathbf{U}} + \nabla \bar{\mathbf{U}}^T) \right]^2 \quad (10)$$

However, the dissipative scales of motion are rectified poorly by LES. In a turbulent flow, the energy from the large resolved structures are passed on to the smaller unresolved structures by an inertial and an effective inviscid mechanism. This is known as energy cascade. Hence, LES employs a sub-grid scale model to mimic the drain related to this energy cascade. Most of these models are eddy viscosity models relating the subgrid-scale stresses (τ_{ij}) and the resolved-scale rate of strain-tensor (\bar{S}_{ij}),

$$\tau_{ij} - (\delta_{ij}/3) = -2\nu_T \bar{S}_{ij} \quad (11)$$

Where, \bar{S}_{ij} is the resolved-scale rate of strain tensor = $(\partial \bar{u}_i / \partial x_j + \partial \bar{u}_j / \partial x_i) / 2$.

In most of the cases it is assumed that all the energy received by the unresolved-scales are dissipated instantaneously. This is the equilibrium assumption, i.e., the small-scales are in equilibrium [7]. This

simplifies the problem to a great extent and an algebraic model is obtained for the eddy viscosity:

$$\mu_{sgs} = \rho C \Delta^2 |\overline{S}| \overline{S}_{ij}, \quad |\overline{S}| = (2 \overline{S}_{ij} \overline{S}_{ij})^{1/2} \quad (12)$$

Here, Δ is the grid size and is usually taken to be the cube root of the cell volume [7]. This model is called as the Smagorinsky model and C is the Smagorinsky coefficient. In the present study, its value has been taken to be 0.2.

IV. NUMERICAL PROCEDURES

A. Numerical scheme and solution algorithm

The three-dimensional compressible Navier-Stokes governing transport equations are discretized through a framework pertaining to finite volume method (FVM) using the SIMPLER algorithm. Here, the turbulent model used for large eddy simulation is Smagorinsky model, because of its simplicity. The spatial derivatives such as Laplacian and convective terms are computed by second order scheme based on Gauss theorem. In addition, the viscous terms are evaluated by second order scheme. Furthermore, the implicit second order scheme is used for time integration. The numerical fluxes are evaluated by applying Sweby limiter to central differencing (CD) scheme, which is a total variation diminishing (TVD) scheme. The central differencing (CD) is an unbounded second order scheme, whereas, the total variation diminishing (TVD) is a limited linear scheme. The established solver is used to predict flow behaviours of the associated flow variables relating to supersonic flow over an open cavity.

B. Choice of grid size, time step and convergence criteria

Figure 2 demonstrates that the computational domain comprises of two regions: upper cavity region and inside cavity region. The grid is refined at the regions near to the wall (where very high gradient is expected) to determine the behaviour of shear layer satisfactorily. A comprehensive grid-independence test is performed to establish a suitable spatial discretization, and the levels of iteration

convergence criteria to be used. As an outcome of this test, the optimum number of grid points used for the final simulation, in the upper cavity region as $360 \times 150 \times 1$ and those of in the inside cavity region as $200 \times 150 \times 1$. Thus, the total number of grid points is 84000. The values of ΔX^+ , ΔY^+ and ΔZ^+ at the leading edge of the cavity are 5, 12.5 and 1.0, respectively. Corresponding time step taken in the simulation is 0.000001 seconds. Though, it is checked with smaller grids of 132000 in numbers, it is observed that a finer grid system does not alter the results significantly.

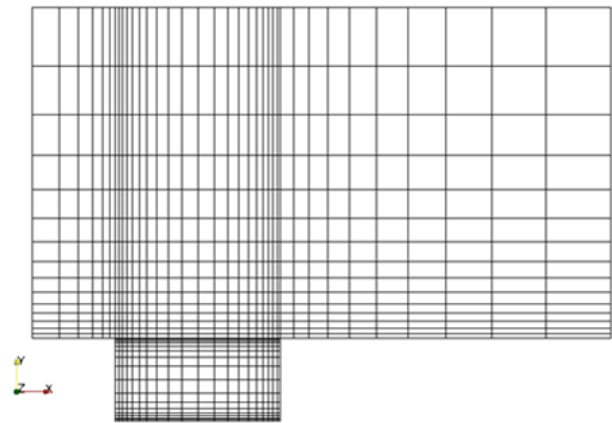


Figure 2. Computational grid of cavity in X-Y Plane.

Convergence in inner iterations is declared only when the condition $\left| \frac{\varphi - \varphi_{old}}{\varphi_{max}} \right| \leq 10^{-4}$ is satisfied simultaneously for all variables, where φ stands for the field variable at a grid point at the current iteration level, φ_{old} represents the corresponding value at the previous iteration level, and φ_{max} is the maximum value of the variable at the current iteration level in the entire domain.

V. RESULTS AND DISCUSSION

A. Coefficient of pressure (Cp) associated with grid Independence test

The spanwise-time averaged-mean coefficient of pressure along the internal cavity is demonstrated in figure 3. Both baseline grid as well as the finer grid have nearly the same coefficient of pressure distributions along the internal cavity. However, the

pressure coefficient for coarse grid is somewhat different from the above-stated two kinds of grids towards the aft wall of the cavity. The variation in the coefficient of pressure is negligible for the smaller grids and hence may be considered to be insensitive to the changes in the grid size. The deviation of the coefficient of pressure between the baseline grid and the finer grid is nearly 0.2 percent.

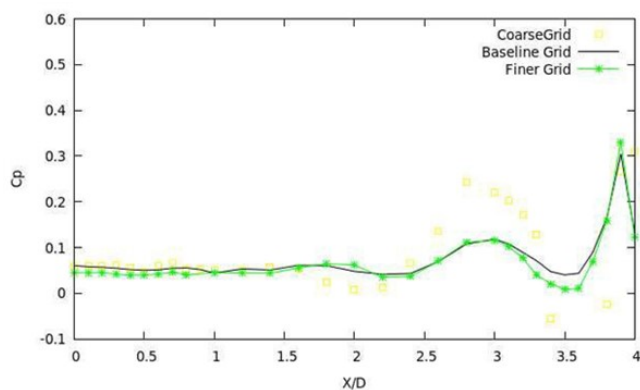


Figure 3. Coefficient of pressure pertaining to the grid independence test of the cavity.

B. Density distributions

The density contours at two different instants of times such as $t = 0.1$ sec and $t = 0.2$ sec are illustrated in figures 4 and 5, respectively. It is pragmatic that a compression wave marching forward arrives at the front wall and then part of the wave is reflected back from the wall. This causes a reflection wave which moves backward. Simultaneously, another feedback compression wave transmits towards the front wall. At the centre part of the cavity, two large vortices are comprehended and these vortices convect towards the trailing edge of the cavity. Large structural vortices strike on the aft wall and at the trailing edge, a very high magnitude of density gradient is prevailed.

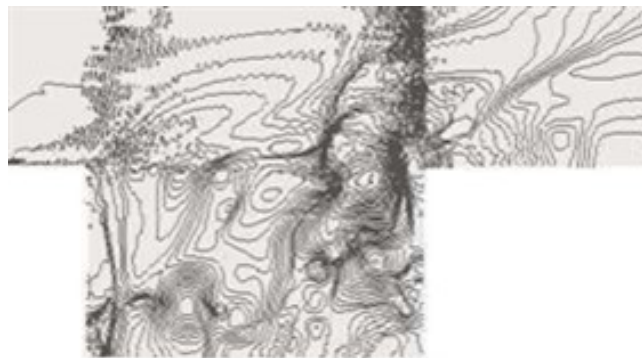


Figure 4. Density contour at time, $t = 0.1$ sec.

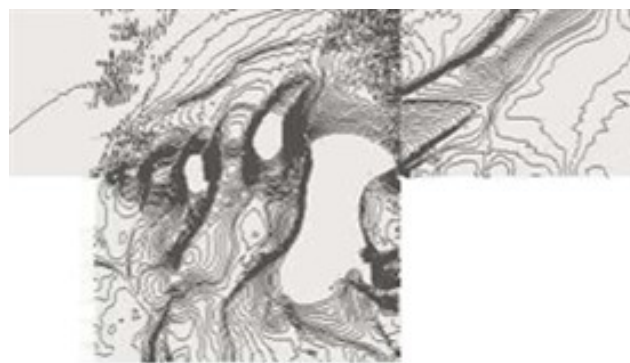


Figure 5. Density contour at time, $t = 0.2$ sec.

The feedback compression wave, which is arrived at the front wall, then arrives at the lip of the leading edge and thus, yields disruption in the shear layer. Another feedback compression wave from the aft wall remains marching towards the front wall. The front vortex, out of the two vortices formed, persuades within the cavity and moves towards the aft wall. A new compression wave is formed at the aft wall edge and transmits upstream.

The shaped reflection wave of feedback compression wave at the front wall as well as the feedback compression from the aft wall come across one another within the cavity. These remain transmitting towards their own direction. The front vortex, as stated previously, strikes on the aft wall, and two shedding vortices act dynamically in the shear layer. Hence, two shocks are shaped, one at the leading edge and the other at the trailing edge.

VI. CONCLUSION

The shedding vortex shaped strikes on the trailing edge lip and is divided into two fragments, one of them convects downstream and the other part travels within the cavity resulting in quite large mass injections. This recirculation flow influences the transmitting direction of the front wall reflection/compression wave moving towards the aft wall. This compression wave remains very weak while it moves toward the aft wall and does not attain high amplitude at the aft wall.

In addition, the density contours of the cavity flows for two more time instants like $t = 0.3$ sec and $t = 0.4$ sec are also demonstrated in figures 6 and 7, respectively. The purpose of the density contour is to show the recirculation regime within the cavity. A very large recirculation regime remains present nearly the aft wall because of the mass injection at very high speed proximate to the trailing edge. A small recirculation regime is also observed at the left bottom corner. The shocks at both leading as well as trailing edges may clearly be realized in the density contours.



Figure 6. Density contour at time, $t = 0.3$ sec.



Figure 7. Density contour at time, $t = 0.4$ sec.

In the current investigational effort, the numerical simulations have been completed for supersonic flow past a 3D open cavity. The cavity possesses length-to-depth ratio of 2 in addition the Mach number of the free-stream is 2.0. The numerical simulations are executed by utilizing LES based on Smagorinsky model for the present open cavity flow. The numerical simulation predictions are captured in the form of both cavity flow-field represented by the density contour and aeroacoustic effect represented by the coefficient of pressure (C_p). The grid independence test pertaining to the coefficient of pressure has also been done. The LES model is very much capable of forecasting all the key flow characteristics of the open cavity flow. Above and beyond, the feedback loop mechanism of the open cavity flow has also been demonstrated. Quite large recirculation is also observed within the open cavity and thus these must be reduced. Conversely, the installation of a spoiler in the form of one-fourth of a cylinder at the leading edge of the open cavity is also planned for future to change the flow characteristics within the open cavity leading to the suppression of the recirculation witnessed within the open cavity as well.

VII. REFERENCES

- [1]. Heller, H. H., Holmes, D. G., & Covert, E. E. (1971). Flow-induced pressure oscillations in shallow cavities. *Journal of sound and Vibration*, 18(4), 545-553.
- [2]. Tam, C. K., & Block, P. J. (1978). On the tones and pressure oscillations induced by flow over rectangular cavities. *Journal of Fluid Mechanics*, 89(02), 373-399.
- [3]. Kaufman, I. I., Louis, G., Maciulaitis, A., & Clark, R. L. (1983). Mach 0.6 to 3.0 flows over rectangular cavities (No. AFWAL-TR-82-3112). Air force wright aeronautical labs wright-patterson AFB, OH.
- [4]. Sweby, P. K. (1984). High resolution schemes using flux limiters for hyperbolic conservation

- laws. SIAM journal on numerical analysis, 21(5), 995-1011.
- [5]. Rizzetta, D. P. (1988). Numerical simulation of supersonic flow over a three-dimensional cavity. AIAA journal, 26(7), 799-807.
- [6]. Anderson, J. D., & Wendt, J. F. (1995). Computational fluid dynamics (Vol. 206). New York: McGraw-Hill.
- [7]. Piomelli, U. (1999). Large-eddy simulation: achievements and challenges. Progress in Aerospace Sciences, 35(4), 335-362.
- [8]. Hamed, A., Das, K., & Basu, D. (2004). Numerical simulations of fluidic control for transonic cavity flows. AIAA Paper, 429, 2004.
- [9]. Li, W., Nonomura, T., Oyama, A., & Fujii, K. (2010). LES Study of Feedback-loop Mechanism of Supersonic Open Cavity Flows. AIAA paper, 5112, 2010.
- [10]. Vijaykrishnan, K. (2014) Unsteady RANS computations of supersonic flow over two dimensional cavity using OpenFOAM-A validation study. AIAA 2014.
- [11]. Sousa, R. G., et al. (2016). Lid-driven cavity flow of viscoelastic liquids. Journal of Non-Newtonian Fluid Mechanics, 234, 129-138, 2016.
- [12]. Tuerke, F., Pastur, L. R., Sciamarella, D., Lusseyran, F., & Artana, G. (2017). Experimental study of double cavity flow. Experiments in Fluids, 76, 2017.